Biosensors and Bioelectronics 167 (2020) 112474

Contents lists available at ScienceDirect

Biosensors and Bioelectronics

journal homepage: http://www.elsevier.com/locate/bios

Urinary exosomal mRNA detection using novel isothermal gene amplification method based on three-way junction

Jeong Moon [a,b], Jaewoo Lim [a,c], Seoyoung Lee [b], Hye Young Son [d,e], Hyun Wook Rho [d], Hongki Kim [a], Hyunju Kang [a], Jinyoung Jeong [f,c], Eun-Kyung Lim [a,c], Juyeon Jung [a,c], Yong-Min Huh [d,g], Hyun Gyu Park [b,**], Taejoon Kang [a,*]

[a] Bionanotechnology Research Center, KRIBB, Daejeon, 34141, Republic of Korea
[b] Department of Chemical and Biomolecular Engineering (BK 21+ Program), KAIST, Daejeon, 34141, Republic of Korea
[c] Department of Nanobiotechnology, KRIBB School of Biotechnology, UST, Daejeon, 34113, Republic of Korea
[d] Department of Radiology, College of Medicine, Yonsei University, Seoul, 03772, Republic of Korea
[e] YUHS-KRIBB Medical Convergence Research Institute, Seoul, 03722, Republic of Korea
[f] Environmental Disease Research Center, KRIBB, Daejeon, 34141, Republic of Korea
[g] Severance Biomedical Science Institute, College of Medicine, Yonsei University, Seoul, 03722, Republic of Korea

ARTICLE INFO

Keywords:
Exosome
RNA
Isothermal gene amplification
Three-way junction
G-quadruplex
Cancer diagnosis

ABSTRACT

Exosomal messenger RNA (mRNA) has emerged as a valuable biomarker for liquid biopsy-based disease diagnosis and prognosis due to its stability in body fluids and its biological regulatory function. Here, we report a rapid one-step isothermal gene amplification reaction based on three-way junction (3WJ) formation and the successful detection of urinary exosomal mRNA from tumor-bearing mice. The 3WJ structure can be formed by the association of 3WJ probes (3WJ-template and 3WJ-primer) in the presence of target RNA. After 3WJ structure formation, the 3WJ primer is repeatedly extended and cleaved by a combination of DNA polymerase and nicking endonuclease, producing multiple signal primers. Subsequently, the signal primers promote a specially designed network reaction pathway to produce G-quadruplex probes under isothermal conditions. Finally, G-quadruplex structure produces highly enhanced fluorescence signal upon binding to thioflavin T. This method provides a detection limit of 1.23 pM (24.6 amol) with high selectivity for the target RNA. More importantly, this method can be useful for the sensing of various kinds of mRNA, including breast cancer cellular mRNA, breast cancer exosomal mRNA, and even urinary exosomal mRNA from breast cancer mice. We anticipate that the developed RNA detection assay can be used for various biomedical applications, such as disease diagnosis, prognosis, and treatment monitoring.

1. Introduction

Exosomes are extracellular vesicles that are released from cells (Pegtel and Gould, 2019). They segregate from many cells as a membrane-enclosed vesicle structure and enter into the bloodstream or other biofluids(Hartjes et al., 2019). Recently, exosomes have emerged as attractive biomarkers for cancer diagnosis and treatment monitoring because exosomes released from tumor cells contain nucleic acids, proteins, and lipids that provide potential information on tumors(Li and Nabet, 2019; Samanta et al., 2018). In particular, cancer exosomes in the urine of a patient have become a promising resource for liquid biopsy, as they can be obtained noninvasively in large quantities(Alvarez, 2014). Among the several cargos in exosomes, cancer-related nucleic acids can accurately reflect tumor profiles(Chen et al., 2019; Guo et al., 2020; Halvaei et al., 2018; Shao et al., 2015). Therefore, analyzing encapsulated genetic molecules after separating exosomes from urine is considered as one of the promising non-invasive approaches for cancer diagnosis and prognosis(Panfoli, 2017; Zhao et al., 2020).

Messenger RNAs (mRNAs) have typically been used as biomarkers in cancer(Xi et al., 2017). They have been conventionally analyzed by quantitative reverse transcription-polymerase chain reaction (qRT-PCR) (Kim et al., 2018; Nolan et al., 2006). Although the qRT-PCR method is

* Corresponding author.
** Corresponding author.
E-mail addresses: hgpark1@kaist.ac.kr (H.G. Park), kangtaejoon@kribb.re.kr (T. Kang).

https://doi.org/10.1016/j.bios.2020.112474
Received 30 May 2020; Received in revised form 21 July 2020; Accepted 22 July 2020
Available online 5 August 2020

highly sensitive, it is time-consuming and needs a heavy instrument for thermal cycling reactions(Bustin, 2000). Moreover, it has limitations related to false-positive results due to primer-dimer and genomic DNA contamination(Zhao et al., 2013). Diverse isothermal gene amplification techniques have been developed as alternative methods of PCR for mRNA detection, such as nucleic acid sequence-based amplification, reverse transcription recombinase polymerase amplification, and reverse transcription loop-mediated isothermal amplification(Abd El Wahed et al., 2013; Compton, 1991; Ocwieja et al., 2015; Zhao et al., 2015). These methods can be carried out at a constant temperature without complicated instruments; however, all of these methods still require the reverse transcription step of mRNA to cDNA, which is error-prone and thus may produce false-positive signals(Hui et al., 2017). Indeed, reverse transcription is a critical step even for the successful qRT-PCR analysis of mRNA(Nolan et al., 2006).

To overcome the problem caused by the reverse transcription step, three-way junction (3WJ) structure-based RNA detection methods were newly developed. Since the methods directly recognize the target RNA molecule through the two single-stranded oligonucleotide probes, the reverse transcription process is unnecessary(Wharam et al., 2001). Moreover, the 3WJ method can be applied to nucleic acid detection systems without considering the length of the nucleic acid and can be combined with various signal amplification systems such as enzyme-linked oligosorbent assay and rolling circle amplification, enabling us to detect RNA sensitively(Lee et al., 2020; Murakami et al., 2012; Wang et al., 2017; Wharam et al., 2001; Zhang et al., 2014). Recently, we developed a 3WJ-induced isothermal amplification (ThIsAmp) reaction and successfully detected nucleic acids with high sensitivity and selectivity. One of the distinctive advantages is to overcome the limitation of the EXPAR system in which the detectable target is a short nucleic acid. However, ThisAmp system still has much room for improvement in respect of applicability to RNA targeting and *in vivo* testing given that RNA molecules are considered important biological molecules in terms of a diagnostic.

Herein, we report a one-step isothermal G-quadruplex amplification reaction that is triggered by 3WJ structure formation with target RNA. The 3WJ structures can only be constructed in the presence of the target RNA sequence, and then multiple signal primers are derived from the 3WJ structures by the repeated reactions of polymerase and nicking endonuclease. The signal primers are subsequently utilized in the specially designed G-quadruplex amplification reaction, producing a large number of G-quadruplex structures. Finally, the amplified G-quadruplex/thioflavin T (ThT) fluorescence signals are measured in real-time, enabling us to detect RNA rapidly and sensitively. We carefully optimized and verified each step of the method; thus, the proposed method was able to detect RNA at a low concentration of 1.23 pM with high specificity. Furthermore, the method was employed to compare mRNA expression levels between normal and breast cancer cells. Most importantly, the sensing performance of this method was demonstrated by using breast cancer cellular exosomal mRNA and even urinary exosomal mRNA from breast cancer mice. The cancer exosomal mRNA was successfully identified using the proposed method, suggesting that the method can be employed for the non-invasive diagnosis of cancer. To the best of our knowledge, this is the first report of real-time exosomal mRNA detection based on isothermal gene amplification. We anticipate that the developed novel RNA detection approach could be used for various biomedical applications, such as disease diagnosis, prognosis, and treatment monitoring. Moreover, considering the development of a rapid and user-friendly diagnostic system is much more required in a resource-poor setting, we believe that the currently proposed method which is fast and facile one-pot RNA detection system has an apparent advantage.

2. Materials and methods

The detailed experimental details are provided in Supplementary Information.

3. Results and discussion

3.1. Principle of isothermal RNA signal amplification using 3WJ-mediated G-quadruplex recycling reaction

Exosomal mRNAs have been considered as valuable biomarkers for liquid biopsy-based disease diagnosis and prognosis(Zhao et al., 2019). Therefore, analyzing the encapsulated mRNA molecule after separating exosomes from body fluids is regarded as a promising non-invasive disease diagnostic method(Castro-Giner et al., 2018; Halvaei et al., 2018). To achieve this goal, we developed a novel RNA detection method by combining 3WJ formation and G-quadruplex recycling reactions. The previous studies using 3WJ formation in conjunction with signal amplification systems were separated into two steps and required an additional initial temperature ramping from 90 to 98 °C(Murakami et al., 2012; Wharam et al., 2001), while the proposed method could proceed in one-step without an initial ramping process. As shown in Fig. 1a, the method allowed us to detect mRNA from cells and exosomes routinely within 30 min.

The principle of isothermal RNA signal amplification using 3WJ-mediated G-quadruplex recycling is illustrated in Fig. 1b. First, 3WJ probes (3WJ-template and 3WJ-primer) were designed to form a 3WJ structure in the presence of the target RNA sequence (Table S1). When the 3WJ structure is constructed with the target RNA (orange), the elongation and nicking reaction are repeated at the 3′ end of the 3WJ-primer (Cycle 1). After the elongation and nicking reactions, many signal primers (red), cleaved short DNA oligonucleotides, are produced. The signal primers then trigger the G-quadruplex amplification reaction. Four-stranded helical structures called G-quadruplex has been widely applied to the detection and monitoring of nucleic acids because a fluorescence signal can be generated by the interaction between G-quadruplex and fluorescent dye, and the signal exhibits excellent G-quadruplex recognition specificity and proportionality(Bhasikuttan and Mohanty, 2015; Lee et al., 2019; Mohanty et al., 2013). In the G-quadruplex amplification reaction, the signal primer hybridizes with the F-template, which contains signal primer binding sequences, nicking endonuclease recognition sequences, and G-quadruplex sequences. When the signal primer binds to the F-template, the extension, cleavage, and strand displacement are repeated continuously in cycles (Cycle 2), producing G-quadruplex sequences (green). To maximize the signal amplification, we designed the G-quadruplex sequence to possess an additional tag sequence (yellow) that is complementary to the 3' end of the 3WJ-template. Consequently, the G-quadruplex products serve as primers for the 3WJ-template, and additional signal primers can be produced without 3WJ structure formation (Cycle 3). As a result, G-quadruplex structures are exponentially generated and produce fluorescence signals as they interact with ThT dye(Mohanty et al., 2013; Xu et al., 2016). With this principle, target RNA can be detected very sensitively because of the synergistic contribution of three cycling reactions (Cycles 1, 2, and 3). Note that the whole series of reaction can be accomplished in a single tube within 30 min after simple mixing of the target RNA sample with the prepared reaction buffers.

3.2. 3WJ probe design to detect human PPP1R1B mRNA

As a proof of concept, we tried to detect synthetic RNA using the gene amplification method based on 3WJ. The synthesized target RNA was 52-bases long and carried the human PPP1R1B mRNA sequence (Table S1). As shown in Fig. 1b and Table S1, the 3WJ-template was designed to include a short signal primer sequence (red) and nicking enzyme Nt.BstNBI recognition site (gray) at the 5′ end. The target-specific region (navy) was next to the 7 bp-complementary sequences to the 3WJ-primer (blue), and additional tag sequences (dT5, yellow) were added at the 3′ end. In addition, the 3′ end was modified into a

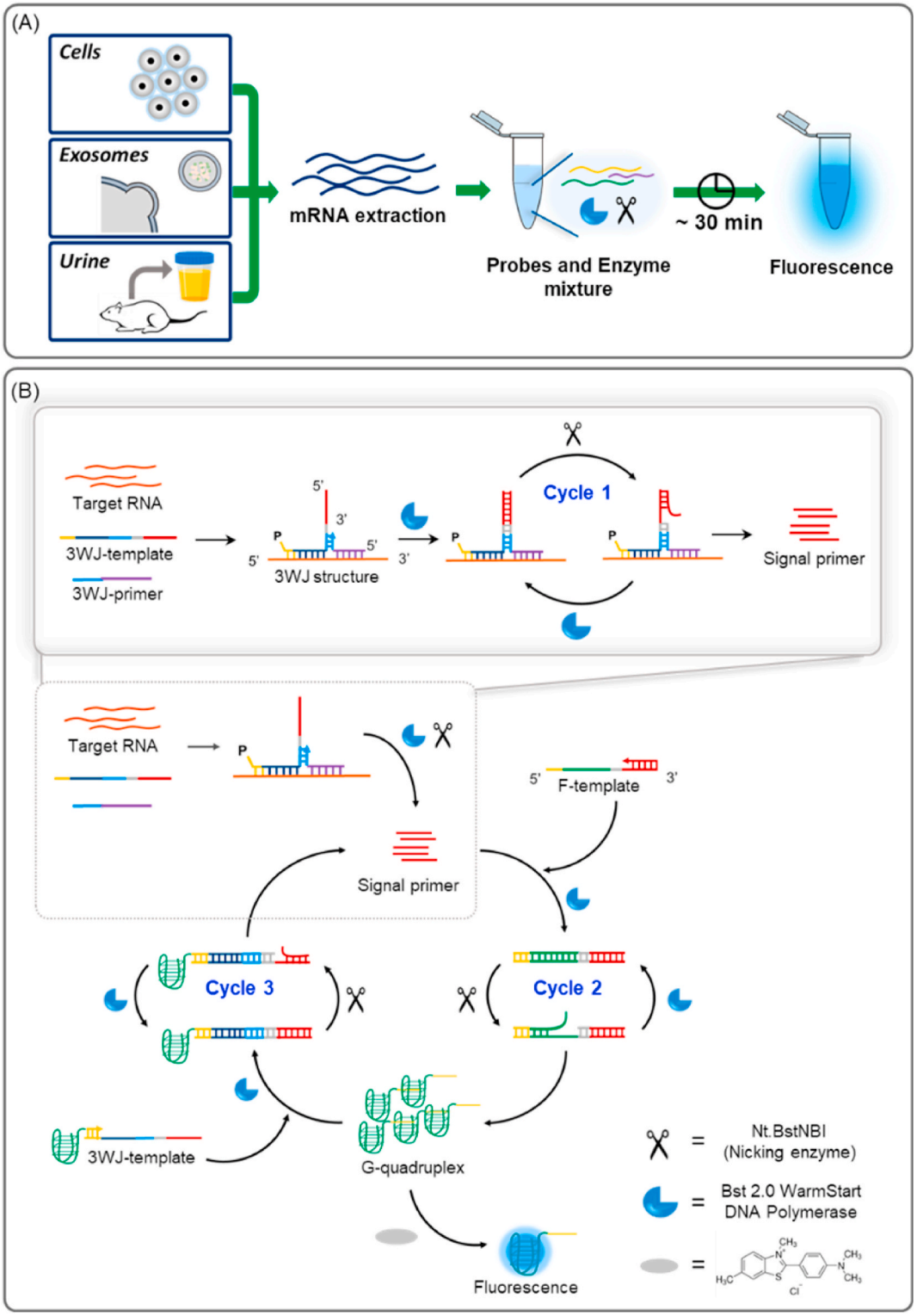

Fig. 1. (A) One-step detection of mRNA extracted from cells, exosomes, and urinary exosomes within 30 min. (B) Principle of RNA detection method based on 3WJ-mediated G-quadruplex recycling reaction.

phosphate functional group to prevent extension in the opposite direction. The 3WJ-primer contained 7 bp-complementary sequences to the 3WJ-template (blue) at the 3′ end and the target-specific region (purple) at the 5’ end. After the design and preparation of the 3WJ-template, 3WJ-primer, and target RNA, melting temperature analysis was conducted using SYBR green I dye to confirm 3WJ formation. When the target RNA was mixed with 3WJ-template and 3WJ-primer, the melting temperature was observed at 70.4 °C (Fig. S1a). This shows that the RNA and 3WJ probes could form a stable structure at the reaction temperature (55 °C). Similar melting temperature results were obtained between the target RNA and either individual 3WJ probe (Figs. S1b and c). However, when the 3WJ-template and 3WJ-primer were mixed, no melting point peak was observed (Fig. S1d), suggesting that no double-stranded structure was formed between the two different 3WJ probes.

For complete 3WJ structure formation, the target RNA, 3WJ-template, and 3WJ-primer should all be required.

Next, we examined whether signal primers can be produced by a combination of elongation and cleavage reactions (Cycle 1). The target RNA and 3WJ probes were mixed and incubated at 55 °C with Bst DNA polymerase and Nt.BstNBI nicking enzyme. After the reaction, the result was analyzed on a 10% polyacrylamide gel (left panel of Fig. 2). When the target RNA molecules were mixed with 3WJ probes, products of about 20-bases long, corresponding to the signal primers, were clearly observed within 10 min. On the other hand, the signal primer band was not observed in the absence of RNA molecules or one of the 3WJ probes. Additionally, the signal primer generation reaction was tested under different enzyme conditions (right panel of Fig. 2). Only when both nicking enzyme and polymerase were mixed with the target RNA and 3WJ probes could the signal primers be produced. This proves that the Cycle 1 step operates well, and thus, signal primers can be produced in the presence of target RNA.

3.3. Feasibility of 3WJ-mediated G-quadruplex amplification reaction

After the formation of the 3WJ structure and the generation of signal primers, the G-quadruplex amplification reaction is triggered. We designed an F-template to contain the signal primer binding region (red in Fig. 1b) and the Nt.BstNBI nicking endonuclease recognition site (gray in Fig. 1b) at the 3′ end for the generation of the G-quadruplex structure. In addition, a 28-bases-long G-quadruplex sequence (green in Fig. 1b) was added at the 5′ end, and an additional sequence containing a complementary sequence to the 3' end of the 3WJ-template (yellow in Fig. 1b) was added next to the G-quadruplex sequence. We tested whether the G-quadruplex sequence can be produced by the Cycle 2 reaction of the F-template and signal primer. The F-template was incubated at 55 °C with the enzyme mixture (Bst DNA polymerase and Nt.BstNBI nicking endonuclease) for 20 min with or without a synthesized 22-bases long signal primer. After incubation, it was analyzed on a 10% polyacrylamide gel. As shown in the left panel of Figs. S2a and a band corresponding to the G-quadruplex was observed only in the presence of the signal primer. Plus, the F-template and signal primer were incubated at 55 °C under the different enzyme mixture conditions for 20 min, and the results indicated that both polymerase and endonuclease were required for G-quadruplex production (right panel of Fig. S2a).

The G-quadruplex sequence generated in the Cycle 2 reaction has an additional tag sequence (yellow in Fig. 1b) that is complementary to the 3' end of the 3WJ-template. Therefore, the G-quadruplex products can act as a primer for the 3WJ-template, and additional signal primers can be produced (Cycle 3). This step further induces the exponential amplification of G-quadruplex structures. We also investigated whether the signal primer can be generated by the Cycle 3 reaction of the 3WJ-template and the G-quadruplex sequence. The 3WJ-template was incubated at 55 °C with the enzyme mixture for 20 min with or without a synthesized 28-bases long G-quadruplex. It was analyzed on the 10% polyacrylamide gel, and a band corresponding to the signal primer was observed only in the presence of G-quadruplex (left panel of Fig. S2b). The right panel of Fig. S2b shows that both polymerase and endonuclease were required for the Cycle 3 reaction.

After the whole RNA sensing reactions, including Cycles 1, 2, and 3, the final G-quadruplex sequences interact with ThT molecules, providing fluorescence signals. ThT can interact with G-quadruplex by the end-stacking mode on the top G-tetrad, resulting in significant fluorescence enhancement(Xu et al., 2016;Khusbu et al., 2018). ThT also exhibits a high recognition specificity for the G-quadruplex structure (Mohanty et al., 2013). We observed noticeable fluorescence signals when the ThT dye was mixed with Cycle 2 reaction solution, including F-template, signal primer, and enzymes (red spectrum in Fig. S3). This result indicated that ThT dye successfully bound to the G-quadruplex structures produced in Cycle 2. When the Cycle 2 reaction could not be carried out, the fluorescence signals were hardly detectable (black, blue, purple, green, and orange spectra in Fig. S3). In addition, we tried to confirm the synergistic signal amplification reactions of Cycles 2 and 3 by measuring the real-time ThT/G-quadruplex fluorescence signals. Fig. 3a shows real-time fluorescence signals observed during Cycle 2 and 3 reactions under several combinations of 3WJ-template and F-template in the presence of signal primer. When the signal primer was mixed with the 3WJ-template, no reaction occurred, and weak fluorescence signals were observed (green curve in Fig. 3a). When the signal primer was mixed with the F-template, a Cycle 2 reaction occurred, and G-quadruplex structures formed. Therefore, the fluorescence signals slightly increased (blue curve in Fig. 3a) compared to the signals of the 3WJ-template (green curve in Fig. 3a). When the signal primer was mixed with F-template and 3WJ-template, the real-time fluorescence signals were significantly increased (red curve in Fig. 3a). This verified that the G-quadruplex was produced in Cycle 2 and then bound to the 3WJ-template, generating a signal primer again and inducing exponential G-quadruplex production. The plot of the quantification cycle value (Cq), defined as the reaction cycle number at which the fluorescence signal intersects the threshold line, also supports that the synergistic reactions of Cycles 2 and 3 provide strongly increased fluorescence signals (Fig. 3b). We also conducted real-time fluorescence measurements during the reactions with several combinations of 3WJ-template and F-template in the presence of G-quadruplex (Fig. 3c). From the mixture of G-quadruplex and F-template structures, weak fluorescence signals were obtained because no reaction occurred (blue curve in Fig. 3c). The mixture of G-quadruplex and 3WJ-template structures provided similar weak fluorescence signals (green curve in Fig. 3c). In this mixture, the G-quadruplex structures bound with the 3WJ-template structures, producing several signal primers (Cycle 3). However, no further reaction proceeded due to the absence of the F-template. Only from the mixture of G-quadruplex, 3WJ-template, and F-template structures could strong fluorescence signals be obtained (red curve in

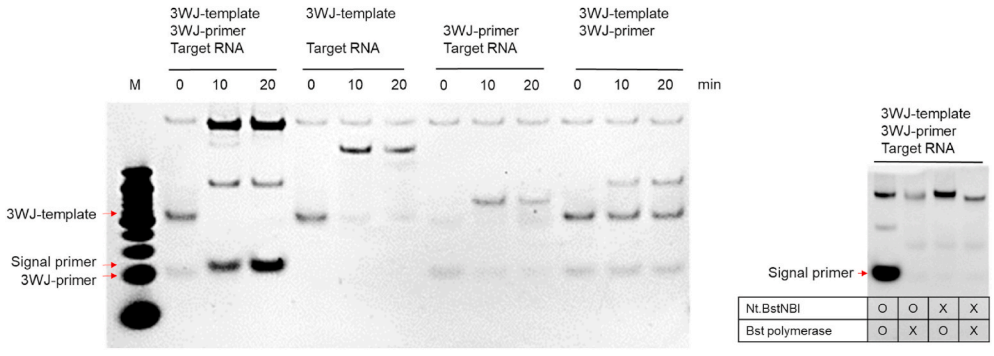

Fig. 2. Polyacrylamide gel analysis of the Cycle 1 reaction. 3WJ-template, 3WJ-primer, and target RNA were mixed in different combinations, and the reaction was conducted with Bst DNA polymerase and Nt.BstNBI nicking endonuclease for 0, 10, and 20 min (left). 3WJ-template, 3WJ-primer, and target RNA were mixed, and the reaction was conducted with different combinations of Bst DNA polymerase and Nt.BstNBI nicking endonuclease for 20 min (right). Lane M is a 10- to 150-bp oligonucleotide marker. [F-template] = 100 nM, [Signal primer] = 50 nM, [3WJ-template] = 50 nM, [3WJ-primer] = 50 nM, [G-quadruplex] = 50 nM, [Bst DNA polymerase] = 1.6 U, and [Nt.BstNBI nicking endonuclease] = 2 U.

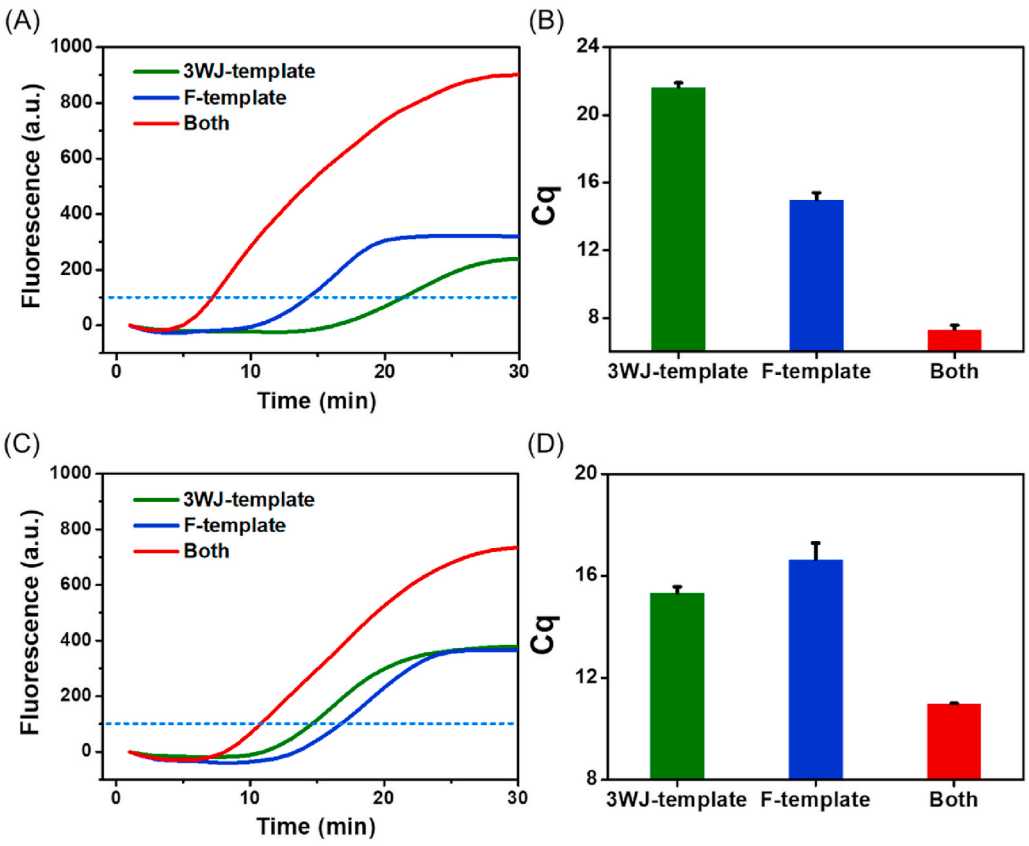

Fig. 3. (A) Real-time fluorescence curves and (B) corresponding Cq values obtained during Cycle 2 and 3 reactions with several combinations of 3WJ-template and F-template in the presence of signal primer. (C) Real-time fluorescence curves and (D) corresponding Cq values obtained during Cycle 2 and 3 reactions with several combinations of 3WJ-template and F-template in the presence of G-quadruplex. [Signal primer] = 1 nM, [G-quadruplex] = 1 nM, [F-template] = 50 nM, [3WJ-template] = 5 nM, [Bst DNA polymerase] = 1 U, and [Nt.BstNBI nicking endonuclease] = 1.6 U.

Fig. 3c). Fig. 3d is the corresponding plot of Cq. The fluorescence results indicated that the signal primer following the G-quadruplex and 3WJ-template reaction could bind to the F-template and produce an additional G-quadruplex sequence. In short, the ThT/G-quadruplex fluorescence signals could be efficiently enhanced by the gene amplification reactions of Cycles 2 and 3.

We further tested the G-quadruplex recycling reactions by using a random-tailed F-template and a random-tailed 3WJ-template (Fig. S4). The results successfully verified that the G-quadruplex recycling reaction was performed by a specially designed G-quadruplex tail sequence. Moreover, after the verification of each cycle in the developed isothermal RNA sensing method, we optimized the concentration conditions of enzymes, 3WJ probes, and F-template respectively. The optimal conditions of enzymes were determined to 1 U of Bst polymerase and 1.6 U of Nt.BstNBI nicking enzyme by comparing the real-time fluorescence curves for the detection of target RNA and control samples (Figs. S5 and 6). Similarly, the concentrations of the 3WJ probes and F-template were optimized to 3 nM and 30 nM, respectively (Fig. S7), and the optimal reaction temperature was also confirmed (Fig. S8).

3.4. Sensitivity and selectivity

As described above, we confirmed that the proposed RNA sensing method could work correctly under the optimized conditions. After that, we evaluated the sensitivity of the RNA detection method by using various concentrations of synthetic PPP1R1B RNA in the range of 1 pM–100 nM. Target RNA was mixed with 3WJ probes (3 nM) and F-template (30 nM) and incubated with the enzyme mixture (1 U of Bst DNA polymerase and 1.6 U of Nt.BstNBI nicking enzyme) at 55 °C. Next, the fluorescence curves were measured in real-time (Fig. 4a), and the plot of the Cq value was obtained (Fig. 4b). The Cq value was linearly dependent on the logarithm (log) of the target RNA concentration in the range of 1 pM–100 nM. The linearly fitted line equation was $y = 2.2681x - 9.8747$ ($R^2 = 0.9901$), where y is the Cq value and x is the RNA concentration. Following the formula LOD = 3 × standard deviation of linear regression/slope, the detection limit was estimated to 1.23 pM. In addition, the fluorescence intensity at the end of the reaction was examined. As shown in Figs. S9a and a gradual increase in fluorescence at 490 nm was observed as the RNA concentration increased from 1 pM to 100 nM. Fig. S9b further shows the plot of relative fluorescence intensity (F/F_0) versus -log [PPP1R1B]. F and F_0 represent the fluorescence intensities at 490 nm in the presence and absence of the target RNA, respectively. Prior isothermal signal amplification strategies for nucleic acid detection have shown comparable results with the currently proposed method through 2 or 3 steps for more than 2 h (Table S2). Whereas, it is worth noting that the developed method could detect the target RNA in a one-step manner within 30 min. Since the fluorescence enhancement of ThT/G-quadruplex is dependent on the G-quadruplex-forming sequences (Faverie et al., 2014) the sensitivity is expected to be improved by using the sequence which has a more efficient fluorescence response to ThT.

Fig. 4c and d indicates the selectivity of the developed RNA sensing approach. For the selectivity evaluation, two kinds of RNA (GAPDH and ERBB2 sequence) and two kinds of non-target ssDNA were employed instead of target PPP1R1B RNA. As shown in Fig. 4c and d, the real-time fluorescence responses of non-target RNAs and ssDNAs were not only nearly the same as the control signal but also much slower than that of the target RNA sample. The fluorescence intensity at the end of the reaction also corresponds to the real-time responses, suggesting a high sequence specificity of this assay (Figs. S9c and d).

3.5. Practical utility

For the application of this method to exosomal mRNA-based disease diagnosis and prognosis, we tried to detect mRNA from human cell lines,

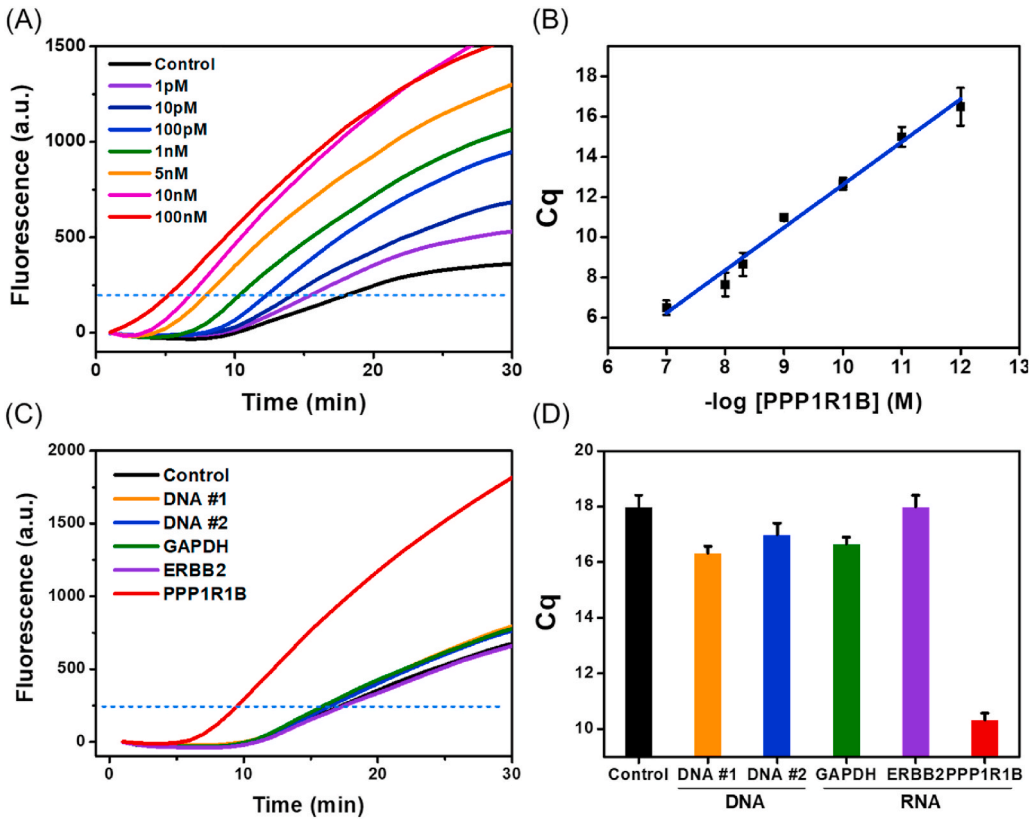

Fig. 4. (A) Real-time fluorescence curves and (B) corresponding Cq values during the detection of PPP1R1B RNA (0, 1, 10, 100 pM, 1, 5, 10, 100 nM). (C) Real-time fluorescence curves and (D) corresponding Cq values during the detection of non-target ssDNAs, and GAPDH, ERBB2, and PPP1R1B RNAs. Error bars were estimated from triplicate tests.

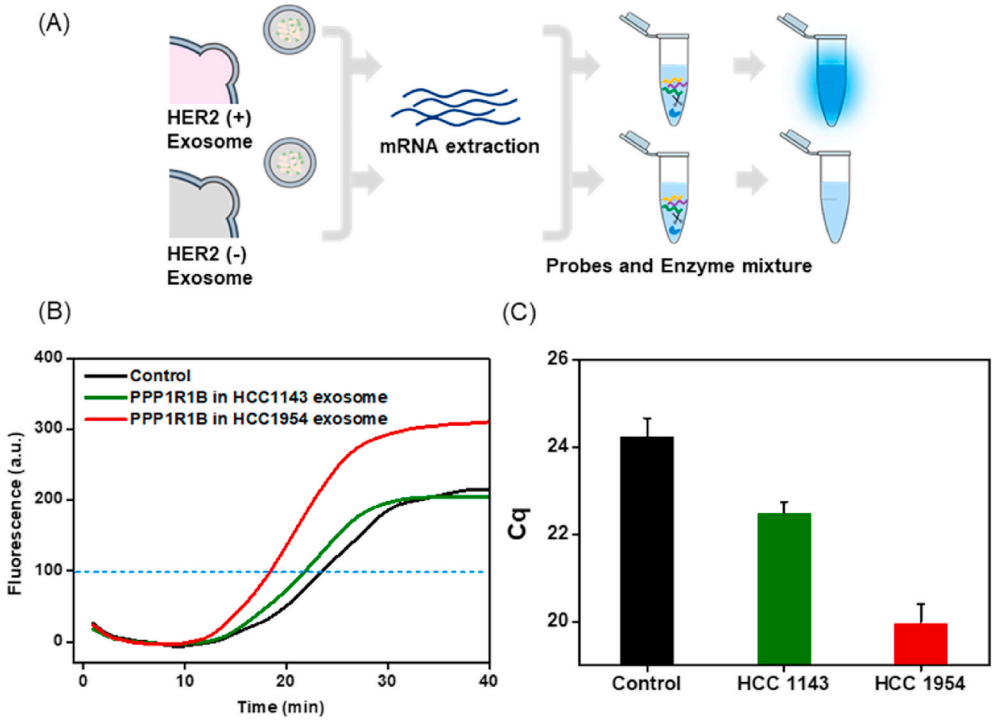

Fig. 5. (A) Schematic illustration of PPP1R1B mRNA detection in exosomes of HCC1143 (HER2 (−)) and HCC1954 (HER2 (+)) cells. (B) Real-time fluorescence curves and (C) corresponding Cq values during the detection of PPP1R1B RNA extracted from the exosomes of HCC1954 and HCC1143 cells. Error bars were estimated from triplicate tests.

exosomes, and urinary exosomes of tumor-bearing mice. First, two different human cell lines (HCC1954 and HCC1143) were prepared for the experiments. HCC1954 cells are HER2-positive, and HCC1143 cells are HER2-negative(Grigoriadis et al., 2012). It is known that the abnormal overexpression of PPP1R1B RNA is associated with the development of various cancers, and specifically that PPP1R1B RNA is elevated in HER2-positive breast cancer cell lines(Avanes et al., 2019; Christenson and Kane, 2014; Kotecha et al., 2019). Therefore, we tried to compare the PPP1R1B RNA expression levels of the HCC1954 and HCC1143 cell lines by using the proposed RNA detection method (Fig. S10a). For the detection of RNA, both HCC1954 and HCC1143 cells were cultured to 10^6 cells/mL, and then their total RNA was extracted. The extracted human mRNA was then analyzed with 3WJ probes and F-template. As a result, the Cq value obtained from the HCC1954 sample was meaningfully lower than that from the HCC1143 sample and the control (Figs. S10b and c). To confirm this result, we analyzed the same samples by using qRT-PCR, and the same result was obtained (Fig. S11). This indicates that the expression level of PPP1R1B mRNA in human cells was successfully analyzed by the proposed method. Second, the mRNA levels in exosomes isolated from the culture medium of HCC1143 and HCC1954 cells were analyzed (Fig. 5a). The cell growth media of both HCC1954 and HCC1143 cells were harvested, respectively, and the exosomes were separated from the media by centrifugation. Subsequently, the exosomal RNAs were extracted, and 5 ng of total exosomal RNA was used for the test. The analysis of exosomal RNA showed a similar RNA expression tendency to the cellular test. The Cq value measured from HER2-positive exosomes was significantly lower than that from HER2-negative exosomes (Fig. 5b and c). These results clearly verified that exosomal mRNA can be identified through the proposed 3WJ probes- and F-template-based reactions.

Last, we tried to analyze the mRNA expression in the urinary exosomes of breast cancer mice. Urine has been traditionally considered a valuable diagnostic medium, and exosomes in urine have recently attracted attention as new biomarker sources because the exosomes in urine contain lipids, mRNAs, non-coding RNAs, DNA, and active proteins, which can provide important information for disease diagnosis and prognosis(Rahbarghazi et al., 2019). In particular, cancer exosomes in urine are regarded as a promising non-invasive diagnostic biomarker source since large quantities can be obtained noninvasively(Panfoli, 2017). For patients, non-invasive liquid biopsies using body fluids may be preferable to tumor tissue biopsies(Boukouris and Mathivanan, 2015). To validate the clinical applicability of the developed RNA sensing method, we prepared a tumor-bearing mouse model and analyzed the mRNA levels in urinary exosomes collected from mouse patients (Fig. 6a). The breast cancer xenograft model was developed by the injection of HCC1954 cells into the mammary fat pad of female mice (total 16 mouse model). Fig. S12a shows representative images of the breast cancer xenograft model mice. Urine from those mice was collected and centrifuged. Next, the exosomes in urine were isolated using the purification system. The isolated exosomes were successfully identified by measuring CD63, one of the exosome marker proteins using western blot assay (Fig. S12). (Curley et al., 2020) After mRNA extraction from the urinary exosome samples, 10 ng of total RNA was prepared, and the PPP1R1B levels were analyzed using the proposed method. Fig. 6c shows the real-time fluorescence curves obtained from the urinary exosomal RNA isolated from HCC1954-derived (red) and healthy (green) mice, respectively. The PPP1R1B mRNA level in urinary exosomes was elevated in mice bearing HER2-positive tumors. Conversely, the PPP1R1B mRNA level of the healthy mouse was similar to that of a blank sample. From the results, it was demonstrated that this novel RNA detection platform could be used for non-invasive cancer diagnosis. We have tried to develop an integrated portable diagnostic

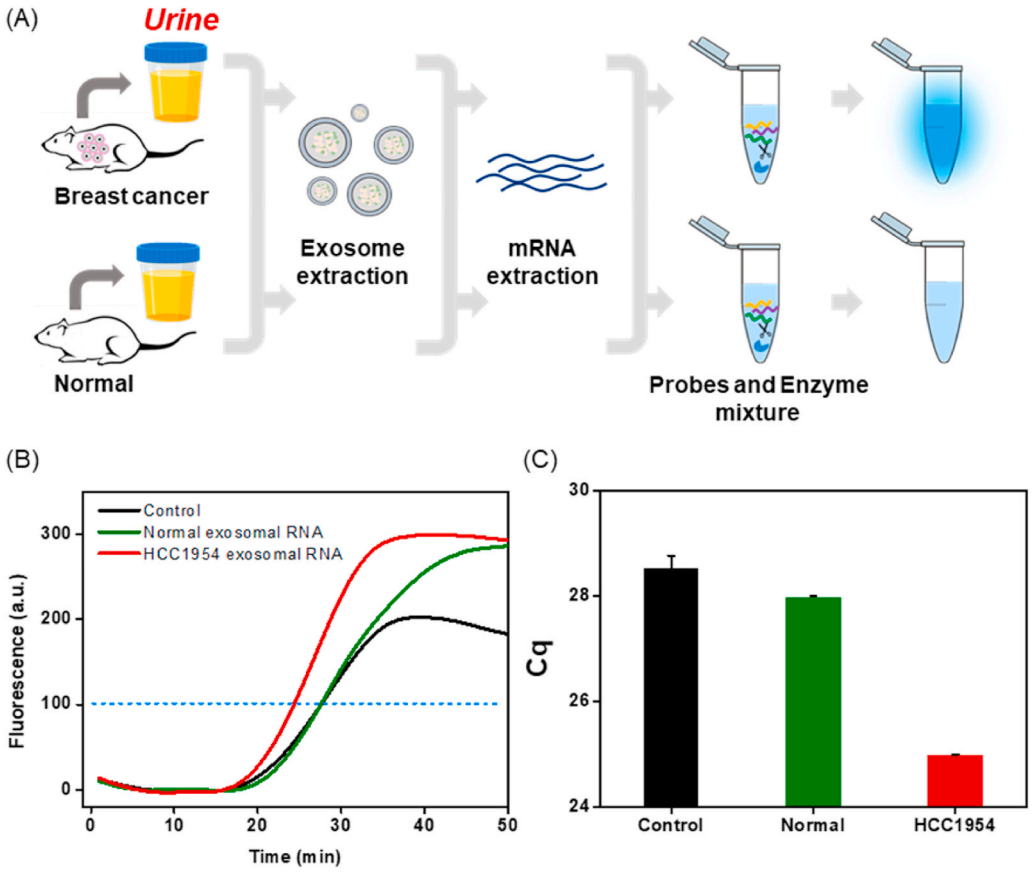

Fig. 6. (A) Schematic illustration of PPP1R1B exosomal RNA detection in mouse urine samples. (B) Real-time fluorescence curves and (C) corresponding Cq values during the detection of PPP1R1B exosomal RNA isolated from healthy control and HCC1954-derived mouse urine samples. Each sample was tested in triplicate.

tool that can separate exosomes from urine samples and detect RNA sequentially based on fluorescence measurement. At present, inconvenient RNA extraction steps are required in this study, not appropriate in a constrained setting. However, we expect that the portable device can simplify the separation and lysis process of exosomes from urine samples, resolving this problem. Concurrently, this rapid one-step RNA detection method would create a synergetic effect when combined with a portable system, especially in a resource-poor setting.

4. Conclusion

In this study, a rapid isothermal G-quadruplex amplification reaction based on 3WJ formation was developed to detect RNA molecules. The strategy described in this manuscript would bring some promising features for biomolecular diagnosis. First, RNA recognition by the 3WJ structure could eliminate the reverse transcription process as well as improved the specificity. Second, the G-quadruplex amplification reaction induced by 3WJ formation efficiently enhanced ThT/G-quadruplex-based fluorescence. This one-step RNA detection method achieved a wide dynamic range and a detection limit of 1.23 pM. Although the sensitivity may be unsatisfactory to some extent compared to other RNA detection methods that take more than 2 h over 2 or 3 steps, this strategy has successfully detected target RNA within 30 min in a one-step manner. Third, it was successfully applied to urinary exosomal mRNA analysis of breast cancer mice. We expect that the proposed method could be widely used for various cancer diagnosis and prognosis tests.

CRediT authorship contribution statement

Jeong Moon: Conceptualization, Methodology, Validation, Investigation, Visualization, Writing - original draft, Writing - review & editing. **Jaewoo Lim:** Validation, Writing - original draft. **Seoyoung Lee:** Conceptualization. **Hye Young Son:** Resources, Writing - original draft. **Hyun Wook Rho:** Resources, Writing - original draft. **Hongki Kim:** Investigation. **Hyunju Kang:** Investigation. **Jinyoung Jeong:** Resources. **Eun-Kyung Lim:** Resources, Data curation. **Juyeon Jung:** Resources. **Yong-Min Huh:** Resources. **Hyun Gyu Park:** Supervision, Writing - review & editing. **Taejoon Kang:** Project administration, Supervision, Writing - original draft, Writing - review & editing.

Declaration of competing interest

The authors declare that they have no known competing financial interests or personal relationships that could have appeared to influence the work reported in this paper.

Acknowledgment

This research was supported by the Center for BioNano Health-Guard funded by the Ministry of Science and ICT of Korea (MSIT) as Global Frontier Project (H-GUARD_2013M3A6B2078950 and H-GUARD_2014-M3A6B2060507), the Bio & Medical Technology Development Program of the National Research Foundation of Korea (NRF) funded by MSIT (NRF-2018M3A9E2022821), the Basic Science Research Program of NRF funded by MSIT (NRF-2019R1C1C1006867), the midcareer Researcher Support Program of NRF funded by MSIT (NRF-2018R1A2A1A05022355), and KRIBB Research initiative Program. J. Moon is the recipient of Global Ph.D. Fellowship (NRF-2019H1A2A1073468).

Appendix A. Supplementary data

Supplementary data to this article can be found online at https://doi.org/10.1016/j.bios.2020.112474.

References

Abd El Wahed, A., Patel, P., Heidenreich, D., Hufert, F.T., Weidmann, M., 2013. PLoS Curr 5.
Alvarez, M.L., 2014. Methods Mol. Biol. 1182, 145–170.
Avanes, A., Lenz, G., Momand, J., 2019. Biochem. Pharmacol. 160, 71–79.
Bhasikuttan, A.C., Mohanty, J., 2015. Chem. Commun. 51 (36), 7581–7597.
Boukouris, S., Mathivanan, S., 2015. Proteonomics Clin. Appl. 9 (3–4), 358–367.
Bustin, S.A., 2000. J. Mol. Endocrinol. 25 (2), 169–193.
Castro-Giner, F., Gkountela, S., Donato, C., Alborelli, I., Quagliata, L., Ng, C.K.Y., Piscuoglio, S., Aceto, N., 2018. Diagnostics 8 (2).
Chen, J., Wu, Y., Fu, C., Cao, H., Tan, X., Shi, W., Wu, Z., 2019. Biosens. Bioelectron. 143, 111619.
Christenson, J.L., Kane, S.E., 2014. Mol. Canc. 13, 192.
Compton, J., 1991. Nature 350 (6313), 91–92.
Curley, N., Levy, D., Do, M.A., Brown, A., Stickney, Z., Marriott, G., Lu, B., 2020. Nanoscale 12 (22), 12014–12026.
Faverie, A.R., Guédin, A., Bedrat, Amina, Yatsunyk, A. Liliya, Mergny, Jean-Louis, 2014. Nucleic Acids Res. 42 (8), e65.
Grigoriadis, A., Mackay, A., Noel, E., Wu, P.J., Natrajan, R., Frankum, J., Reis-Filho, J.S., Tutt, A., 2012. BMC Genom. 13, 619.
Guo, Q., Yu, Y., Zhang, H., Cai, C., Shen, Q., 2020. Anal. Chem. 92 (7), 5302–5310.
Halvaei, S., Daryani, S., Eslami, S.Z., Samadi, T., Jafarbeik-Iravani, N., Bakhshayesh, T. O., Majidzadeh, A.K., Esmaeili, R., 2018. Mol. Ther. Nucleic Acids 10, 131–141.
Hartjes, T.A., Mytnyk, S., Jenster, G.W., van Steijn, V., van Royen, M.E., 2019. Bioengineering (Basel) 6 (1), 7.
Hui, W., Honghong, W., Xinrui, D., Xiangdong, W., Yuanyuan, S., Zhengping, L., 2017. Sensor. Actuator. B Chem. 252, 215–221.
Khusbu, F.Y., Zhou, X., Chen, H., Ma, C., Wang, K., et al., 2018. Trends Analyt Chem 109, 1–18.
Kim, H.Y., Li, T., Jung, C., Fu, R., Cho, D.-Y., Park, K.S., Park, H.G., 2018. RSC Adv. 8, 37391–37395.
Kotecha, S., Lebot, M.N., Sukkarn, B., Ball, G., Moseley, P.M., Chan, S.Y., Green, A.R., Rakha, E., Ellis, I.O., Martin, S.G., Storr, S.J., 2019. Sci. Rep. 9 (1), 16987.
Lee, C.Y., Kim, H., Park, K.S., Park, H.G., 2019. Anal. Chim. Acta 1060, 30–44.
Lee, S., Jang, H., Kim, H.Y., Park, H.G., 2020. Biosens. Bioelectron. 147, 111762.
Li, I., Nabet, B.Y., 2019. Mol. Canc. 18 (1), 32.
Mohanty, J., Barooah, N., Dhamodharan, V., Harikrishna, S., Pradeepkumar, P.I., Bhasikuttan, A.C., 2013. J. Am. Chem. Soc. 135 (1), 367–376.
Murakami, T., Sumaoka, J., Komiyama, M., 2012. Nucleic Acids Res. 40 (3), e22.
Nolan, T., Hands, R.E., Bustin, S.A., 2006. Nat. Protoc. 1 (3), 1559–1582.
Ocwieja, K.E., Sherrill-Mix, S., Liu, C., Song, J., Bau, H., Bushman, F.D., 2015. PloS One 10 (2), e0117852.
Panfoli, I., 2017. Transl. Cancer Res. S1389–S1393.
Pegtel, D.M., Gould, S.J., 2019. Annu. Rev. Biochem. 88, 487–514.
Rahbarghazi, R., Jabbari, N., Sani, N.A., Asghari, R., Salimi, L., Kalashani, S.A., Feghhi, M., Etemadi, T., Akbariazar, E., Mahmoudi, M., Rezaie, J., 2019. Cell Commun. Signal. 17 (1), 73.
Samanta, S., Rajasingh, S., Drosos, N., Zhou, Z., Dawn, B., Rajasingh, J., 2018. Acta Pharmacol. Sin. 39 (4), 501–513.
Shao, H., Chung, J., Lee, K., Balaj, L., Min, C., Carter, B.S., Hochberg, F.H., Breakefield, X.O., Lee, H., Weissleder, R., 2015. Nat. Commun. 6, 6999.
Wang, X., Wang, H., Liu, C., Wang, H., Li, Z., 2017. Chem. Commun. 53 (6), 1124–1127.
Wharam, S.D., Marsh, P., Lloyd, J.S., Ray, T.D., Mock, G.A., Assenberg, R., McPhee, J.E., Brown, P., Weston, A., Cardy, D.L., 2001. Nucleic Acids Res. 29 (11). E54-E54.
Xi, X., Li, T., Huang, Y., Sun, J., Zhu, Y., Yang, Y., Lu, Z.J., 2017. Non-coding RNA 3 (1).
Xu, S., Li, Q., Xiang, J., Yang, Q., Sun, H., Guan, A., Wang, L., Liu, Y., Yu, L., Shi, Y., Chen, H., Tang, Y., 2016. Sci. Rep. 6, 24793.
Zhang, Q., Chen, F., Xu, F., Zhao, Y., Fan, C., 2014. Anal. Chem. 86 (16), 8098–8105.
Zhao, J., Liu, C., Li, Y., Ma, Y., Deng, J., Li, L., Sun, J., 2020. J. Am. Chem. Soc. 142 (11), 4996–5001.
Zhao, Y., Chen, F., Li, Q., Wang, L., Fan, C., 2015. Chem. Rev. 115 (22), 12491–12545.
Zhao, Y., Zhou, L., Tang, Z., 2013. Nat. Commun. 4, 1493.
Zhao, Z., Fan, J., Hsu, Y.S., Lyon, C.J., Ning, B., Hu, T.Y., 2019. Lab Chip 19 (7), 1114–1140.